Local Control of Parity and Charge in Nanoscale Superconducting Lead Islands

Stefano Trivini[1,*,†] Jon Ortuzar[1,*,‡] Katerina Vaxevani[1], Beatriz Viña-Bausá[1],
F. Sebastian Bergeret[2,3] and Jose Ignacio Pascual[1,4,§]

[1]*CIC nanoGUNE-BRTA, 20018 Donostia-San Sebastián, Spain*
[2]*Centro de Física de Materiales CFM-MPC) Centro Mixto CSIC-UPV/EHU, E-20018 Donostia-San Sebastián, Spain*
[3]*Donostia International Physics Center DIPC), 20018 Donostia-San Sebastian, Spain*
[4]*Ikerbasque, Basque Foundation for Science, 48013 Bilbao, Spain*

Small superconducting islands can exhibit charge quantization, where Coulomb interactions compete with Cooper pairing. Using scanning tunneling spectroscopy, we probe this interplay by measuring the charging energy E_C) and the pairing energy   ) of individual Pb nanoislands. Below a critical island size, where $E_C > $, we observe a crossover between even and odd parity ground states. By applying controlled voltage pulses, we continuously tune the island s electrostatic potential and map the full charge-parity landscape. These results demonstrate tunable superconducting ground states, offering a potential platform for qubit design and control.

Single-electron tunneling through a metallic nanoparticle capacitively coupled to two electrodes involves a Coulomb charging energy, E_C, determined by the capacitance of the junctions. In sufficiently small systems, E_C can exceed the thermal energy, making it experimentally measurable [1 6]. This energy barrier gives rise to sequential electron tunneling and underlies the operation of single-electron transistors SETs) [4,7]. In contrast to the repulsive nature of Coulomb interactions, superconducting correlations introduce an effective attractive interaction, characterized by the superconducting gap   , which favors the formation of a Cooper-pair ground state [7 11]. When such correlations are present, as in a superconducting SET, the competition between E_C and   fundamentally modifies the standard SET response to a gate voltage, leading to a transition from single-electron to a two-electron periodic behavior [9,12,13].

A particularly rich regime emerges when the charging energy E_C and the superconducting gap   become comparable and compete in setting the ground-state parity. On one hand, pairing correlations weaken as the mean level spacing increases [6,14]; on the other, localized Cooper pairs remain protected by a parity gap modulated by the combined effects of E_C and   [15]. However, since both mechanisms lead to a gap in the density of states, disentangling their respective roles becomes experimentally challenging. Resolving this competition is essential for

understanding the breakdown of superconductivity [15] and the emergence of insulating phases in nanoscale systems [16,17].

Here we demonstrate full electrostatic control over the parity of the superconducting ground state in individual Pb islands on graphene. Using scanning tunneling spectroscopy STS), we access the regime where pairing and charging energies are comparable, and show that even-parity and odd-parity superconducting states can coexist and be reversibly tuned via gating potentials. The superconducting gap increases with decreasing island size, signaling the onset of Coulomb blockade. By tracking the gap evolution under magnetic field, we disentangle the contributions of pairing   ) and charging energy E_C), and identify a critical radius below which $E_C > $. In this regime, odd-parity ground states emerge when an excess charge of $\pm e$ is added to the island. We induce such transitions by applying voltage pulses with the STM tip, effectively gating the islands potential as in three-terminal geometries. These odd-parity states exhibit a characteristic magnetic-field-induced reopening of the gap, enabling their identification. The demonstrated control over   , E_C, and the local potential opens new routes to engineer parity-based superconducting devices and probe the breakdown of Cooper pairing at the nanoscale.

Description of the system We used graphene grown on a SiC single crystal [18,19] as a substrate, and deposited a ~ 1 ML amount of lead at room temperature and under ultrahigh vacuum. Lead forms flat, threefold symmetric islands [20 22] [Fig. 1 a)], lying in direct contact with graphene [23,24], with effective radii $r_{\text{eff}} = (\text{area}/$ $)^{1/2}$ from 5 nm to more than 40 nm, and heights h) from 3 to 15 nm.

*These authors contributed equally to this work.
†Contact author: stefano.trivini@gmail.com
‡Contact author: jon.ortuzar.a@gmail.com
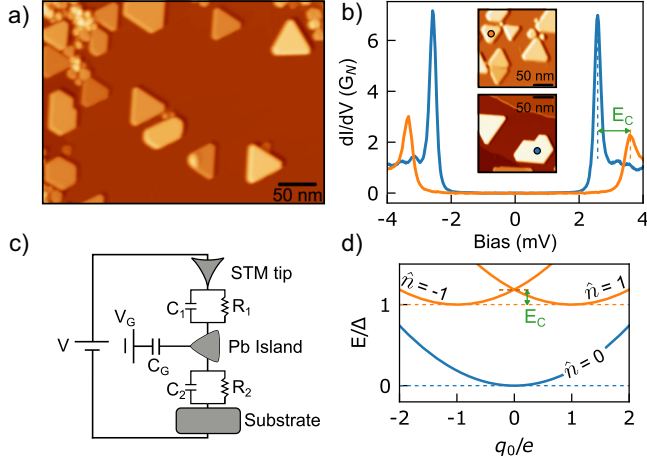§Contact author: ji.pascual@nanogune.eu

FIG. 1. a) STM image of Pb islands on graphene. b) STS on a large $r_{eff} = 39.2$ nm, $h = 4.2$ nm, blue) and small $r_{eff} = 21.7$ nm, $h = 14.1$ nm, orange) island marked in the insets. The conductance is normalized to G_N, the normal state conductance. A finite E_C causes a larger gap in the smaller island. c) DBTJ circuit modeling the tip-island-sample geometry. d) Eigenstates of the DBTJ Hamiltonian, dashed lines for $E_C =$, in blue the even states and orange the odd states. STS @ R = 10 M Ω; STM @ V = 400 mV, I = 20 pA.

At the base temperature of our STM 1.2 K [25]), islands with $r_{eff} > 3$ nm show a superconducting ground state similar to bulk lead, similar to previous works [21,22]. Differential conductance dI/dV) spectra on these islands [e.g., blue curve in Fig. 1 b)] display a BCS-like gap with symmetric coherence peaks. We use Pb-coated superconducting tips with $_t \sim 1.3$ meV to enhance our energy resolution. The coherence peaks appear at $ + _t \sim 2.6$ meV, resulting in a ≈ 1.3 meV for the island, close to the bulk value of lead $_{Pb} = 1.35$ meV). In contrast, smaller islands exhibit significantly larger spectral gaps, as shown in Fig. 1 b) for an $r_{eff} \sim 21.7$ nm island, with a gap of ~ 3.5 meV. The larger gap is consistent with the existence of a charging energy E_C due to Coulomb effects [26,27].

To account for Coulomb blockade effects in the electronic transport through small superconducting islands, we use the double-barrier tunneling junction DBTJ) model sketched in Fig. 1 c). The Pb islands are capacitively coupled to the superconducting tip and the proximitized graphene sample, and their Hamiltonian contains the two main energy scales E_C and [7,8,11,28]:

$$H = H_S + H_C \tag{1}$$

$$H_S = \frac{1 \quad (\quad 1 \quad ^n}{2} \tag{2}$$

$$H_C = \frac{(n \quad q /e \; ^2}{2C} e^2 = E_C(n \quad q /e \; ^2 \tag{3}$$

where H_S accounts for the superconducting pairing, H_C considers the effect of charging the island, and $C = C_1 + C_2$ is the sum of tip-island and island-sample junction capacitances. The full DBTJ model includes the tunneling Hamiltonian from the island to the superconducting electrodes see Supplemental Material for additional details [29]). The superconducting pairing term H_S adds the energy cost of a quasiparticle excitation only for an odd number of electrons in the island [12,13,44 46]. In STM $C_1 \ll C_2$, [24,47,48], therefore the charging energy $E_C \sim e^2/2C_2$ depends mainly on the island-substrate capacitance. The magnitude of E_C is generally negligible for large islands, but becomes sizable as C_2 decreases for small islands. In this case, changes of the integer charge in the island n upon electron transfer have an energy cost E_C. This value can be tuned by an electrostatic gate potential V_G, represented in Eq. 3) as a residual fractional) charge $q = V_G C_G$ [8].

The eigenvalues of Eq. 1) in Fig. 1 d) describe parabolic bands $E_n(q$ shifted in q by one elementary charge e. Superconducting pairing raises the parabolas for odd charge states orange) by relative to even ones blue). At $q =$, exciting a quasiparticle in the island requires both the pairing energy and the charging energy E_C, so the spectral gap reflects their combined effect [16]. As both depend on island size, separating their contributions is nontrivial.
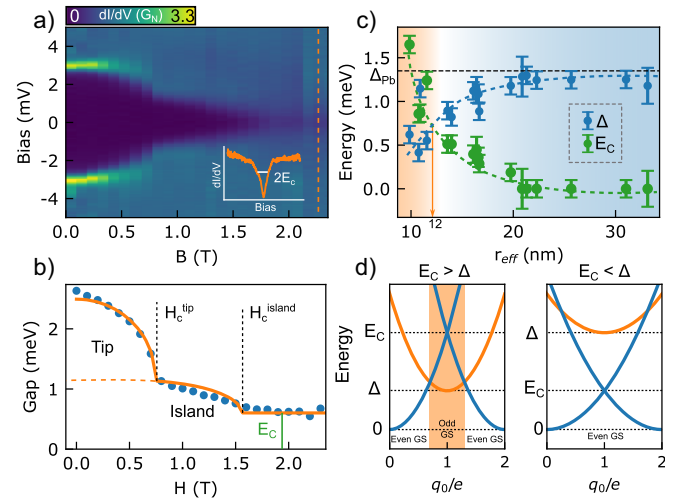

FIG. 2. a) Evolution of the spectral gap with an out-of-plane magnetic field on a $r_{eff} = 15.9$ nm, $h = 15.5$ nm island. The dashed line marks the dI/dV spectrum of the bare Coulomb gap in the inset. b) Gap values blue dots) extracted by DBTJ fits to panel a); the orange curve results from the model in Supplemental Material [29] that captures the sequential closing of the tip and sample gaps, yielding E_C at high fields. c) Extracted values of and E_C as a function of island size, with crossing at $r_c \sim 12$ nm. d) DBTJ eigenstates for $E_C >$ and $E_C <$ as a function of the residual charge q . For $E_C >$ $r_{eff} < 12$ nm), an odd parity ground state GS) emerges around $q \sim \pm e$.

We address this by applying an external magnetic field B and monitoring the evolution of the superconducting gap. As shown in Fig. 2 a) for an island with effective radius $r_{\text{eff}} = 15.9$ nm, both the tip and island superconducting gaps gradually close with increasing B, while E_C remains field-independent. The extracted gap and the theoretical fit appear in Fig. 2 b) details of the fit in Supplemental Material [29]). Starting from a zero-field gap of 2.6 mV, the tip gap $_t$) closes first at a critical field of $B_c^{\text{tip}} \sim .8$ T verified by measurements on bulk-like islands), followed by the island gap) at $B_c^{\text{island}} \sim 1.5$ T details in Supplemental Material [29]). Thus, the remaining gap observed at higher fields [inset of Fig. 2 a)] corresponds exclusively to the charging energy E_C [49].

To reveal the size dependence of E_C and , we applied this procedure to 18 islands with r_{eff} from 10 nm to 35 nm. As shown in Fig. 2 c), E_C is negligible for large islands but increases significantly with decreasing island size. This dependence originates from the capacitance of the island-graphene interface, specifically $C_2 \propto r_{\text{eff}}^2$.

In contrast, the superconducting gap) of the islands decreases as the island size shrinks, reflecting weakened superconducting correlations due to the increasing mean level separation δ) arising from confinement [27] more details about δ in Supplemental Material [29]). The plot in Fig. 2 c) outline a transition to a regime where the charging energy exceeds for island sizes below the critical radius $r_c \sim 12$ nm. In this regime, ground states with odd electron

number one extra quasiparticle) become accessible for an excess charge close to $q = \pm e$ in the island, as depicted in the DBTJ model of Fig. 2 d) [4,44].

Locally gating the Pb islands with voltage pulses In contrast to typical particle-hole symmetric spectra of superconductors, islands with effective radius $r_{\text{eff}} < 25$ nm frequently exhibit coherence dI/dV peaks with bias-asymmetric positions and intensities [e.g., as in the spectrum of Fig. 3 a)]. Such asymmetric spectra originate from a finite electrostatic gate potential V_G, which enters as a nonzero fractional residual charge q in the DBTJ model of Eq. 3) [5]. As shown in the diagram of Fig 3 b), in the presence of Coulomb effects, deviations from the symmetric case $q = $) lead to unequal energy costs for adding $n = +1$), excitation labeled α, or removing an electron $n = 1$), excitation labeled α. This imbalance shifts the coherence peaks depending on the bias polarity, revealing built-in electrostatic potentials at the island graphene interface.

Controllably gating surface-supported objects has long been a challenge in STM experiments [50]. In the Pb/graphene system, we could controllably modify the excess charge q of small islands by applying controlled bias pulses with the STM tip [51]. As shown in Fig. 3 a) upper panel), repeated bias pulses at increasing voltage amplitude, spanning in the range from 3 V to 3 V, induce reproducible changes in the spectral shape, associated to gradual variations of the residual charge q by more than
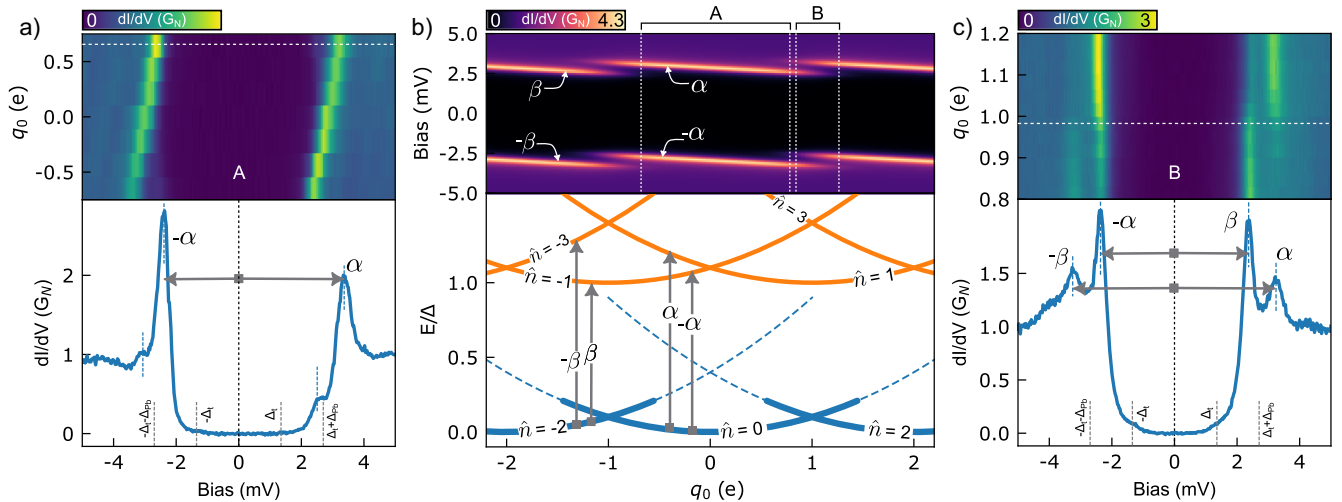

FIG. 3. a) bottom) Differential conductance on a Pb island with $r_{\text{eff}} = 26.8$ nm, $h = 14.3$ nm, and $q \sim .75e$. We label α the dominant resonances occurring at asymmetric energy positions. top) Excess charge dependence map of the island, obtained by consecutive bias pulsing. Each dI/dV spectrum is measured after a bias pulse between 1 and 3V with feedback off at $I = 5$ pA, measuring transient currents of up to 100 nA. b) bottom) Eigenstates of the DBTJ Hamiltonian depending on the electron number n and on the excess charge q. Around $q = $, we indicate with vertical arrows the transitions $\pm\alpha$ visible in the dI/dV of panel a). Close to $q = e$, the ground state population is a mixture of $n = 2$ and the $\pm\beta$ transitions become possible. top) Calculated dI/dV with the DBTJ model as a function of the excess charge, q, with parameters: $= _t = 1.35$ mV, $\Gamma = \Gamma_t = 8$ uV, $C_1 \approx$, $C_2 = 48$ aF, $R_1 = 1 * R_2$, T = 1.3 K. Two regions are highlighted to compare with the corresponding experimental maps. c) bottom) Differential conductance on a Pb island with $r_{\text{eff}} = 15$ nm, $h = 4.1$ nm, at $q \sim e$, showing symmetric excitations labeled α and β. top) Excess charge dependence map of the island around the point $q \sim e$ acquired similarly to the one in panel a).

one electron charge see Supplemental Material for details [29]). Using this gating method, we acquired gate-dependent spectral maps covering different regions of accumulated charge in the islands. The spectral map in Fig. 3 a) shows coherence peaks of a small island shifting markedly after pulses, with unmodified superconducting gap width. This proves that the island s spectral asymmetry arises from a net local gating q , which is modified after each voltage pulse in the window $\sim \pm e$.

The spectral map in Fig. 3 c), showing four dI/dV peaks with varying intensity and position, indicates that the island is near an odd value of residual charge. This behavior is well captured by the DBTJ model in Fig. 3 b), which predicts a degeneracy of the $n =$ and $n =$ 2 ground states at $q =$ e, as well as particle-hole symmetric excitations to the $n =$ 1 and the $n =$ 3 states. From the $n =$ 2 ground state, an additional electron hole) excitation labeled β to $n =$ 1 or β to $n =$ 3) becomes now accessible, accounting for a second pair of excitation peaks close to $q =$ e. The simultaneous observation of α and β coherence peaks with gradually changing amplitude around the crossing of the degeneracy point is attributed to thermal population of both even-parity ground states see Supplemental Material [29]). This agreement enables a direct and accurate determination of odd residual charge states in islands and confirms the persistence of their paired ground states for sizes above the critical effective radius r_c.

Local mapping of the ground state charge As it has been previously shown [21], lead islands can be repositioned around the graphene surface through lateral manipulation with the STM tip. After their movement, we often observe changes or even reversals of spectral asymmetry see Supplemental Material [29]), likely due to localized charges or built-in potential gradients in the substrate [50,51]. This suggests that the island s residual charge is sensitive to variations of the electrostatic landscape of the surface and could be used as a sensor for point charges.

Figure 4 illustrates this concept for a $r_{\rm eff} \sim 21.2$ nm island with ground state at the transition between $n =$ and $n =$ 2, as determined by its spectrum in Fig. 4 b). Two dI/dV peaks at positive and negative bias are consistent with a residual charge of $q \sim$ e. However, as shown in the spectral profile in Fig. 4 c), the intensity and, weakly, the alignment) of the four peaks changes with the position along the center of the island. This evolution resemble the spectral changes with q shown in Fig. 3 c), thus suggesting an inhomogeneous electrostatic potential at the island-graphene interface.

To map the potential landscape, we measured the spatial distribution of the four spectral peaks $\pm \alpha$ and $\pm \beta$ across the island using a grid of STS measurements [within the dashed triangle in Fig. 4 a)]. The radial distribution of peak amplitudes shown in Fig. 4 d) suggests the presence of a point charge near one of the island s corners. The β transitions, representing excitations from the ground state
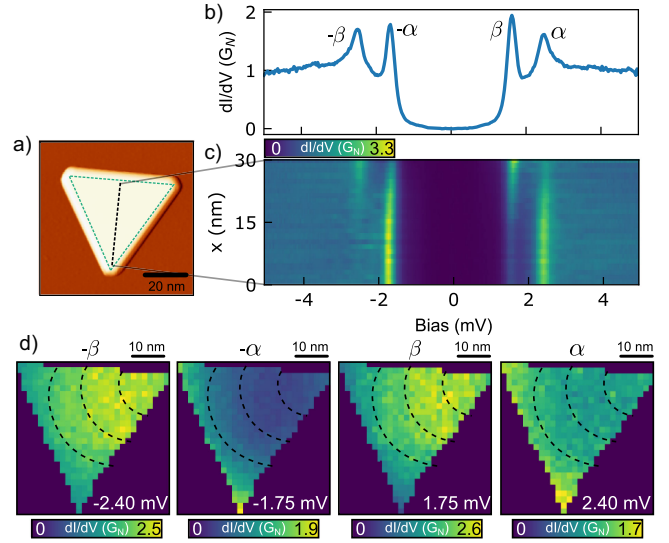

FIG. 4. a) Topographic image of an island with $r_{\rm eff} =$ 21.2 nm, $h = 17.7$ nm. b) Measured dI/dV spectrum on the island with the symmetric resonance labeled $\pm \alpha$ and $\pm \beta$ indicating $q \sim e$. c) Spatial dependence of the LDOS along the black dashed line in panel a). d) Constant energy cuts at $\pm \alpha$ and $\pm \beta$ of a spectral grid acquired over a triangular region on the island in panel a). The radial dashed line indicates the shape of the charge puddle induced in graphene, which modulates locally the excess charge.

with a Cooper pair less $2e$ e and $2e$ $3e$), are strongest toward the upper right corner and fade toward the center. In contrast, $\pm \alpha$ peaks, corresponding to the e and e transitions, are more intense near the left edge. The predominance of the $q =$ $2e$ ground state $\pm \beta$ excitations) in the right corner likely results from the localization of a negative point charge in this region. Such static charge puddles are common in graphene on insulating substrates and can be created, neutralized, or reversed by applying STM voltage pulses [50]. Here, their field acts as a local gate, tuning the island s residual charge.

The doubly peaked gapped spectrum is a hallmark of the persistence of a superconducting paired) ground state in small islands with electrostatic potentials near the $q =$ e point. As shown in the DBTJ simulations in Figs. 5 a) and 5 b), the separation between the two excitations increases with E_C, i.e., inversely with island size, and the outer peak disappears at the crossing $E_C =$. This marks the transition to an odd-parity ground state for $q =$ e, characterized by a single gap of width E_C . In this regime, the remanent electron pairing partially compensates for Coulomb correlations. A distinctive behavior of such odd-parity state is the evolution of its gap with magnetic field H [52]. As superconductivity is suppressed, the gap widens until the bare Coulomb blockade gap emerges [right side of Fig. 5 b)].

This peculiar behavior is demonstrated in Figs. 5 c) and 5 d) for an island with $r_{\rm eff} = 9.5$ nm, smaller than the
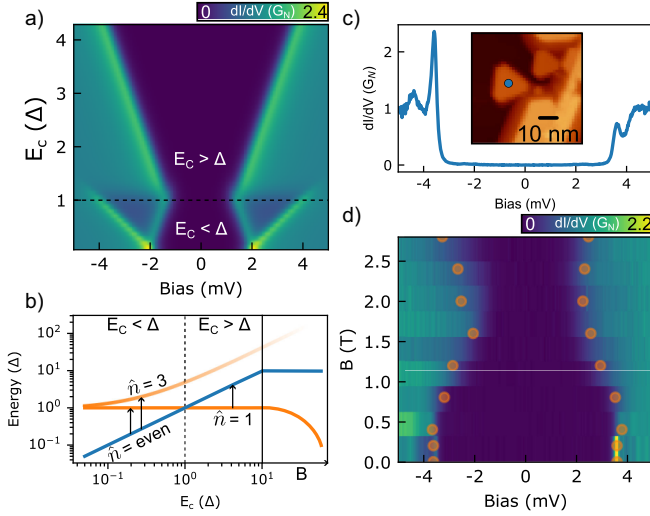
FIG. 5.   a) Calculated LDOS map varying the excess charge. The even parity ground state region with $E_C <$ is separated by a dashed line from the odd parity ground state region with $E_C >$. parameters: $=$ .65 mV, $_t = 1.35$ mV, $\Gamma = \Gamma_t = 18$ uV, $C_1 \approx$, C_2 from 1600 aF to 26 aF, $R_1 = 1$ $* R_2$, T = 1.3 K) b) Ground and excited states increase the charging energy. In the right part of the scheme, we sketch the effect of the magnetic field, which, in an odd parity ground state, opens the energy gap. c) Spectrum on a island with $r_{eff} = 9.5$ nm, $h = 2.7$ nm, with gap ~3.8 mV. d) Magnetic field dependence of the LDOS measured on the same island. The orange dots are fits of the gap magnitude, which initially decreases, due to the closing of $_t$ and increases at higher fields, indicating an odd parity ground state. The asymmetric opening is due to a slight shift from the $q = \pm e$ point.

critical radius $r_c \sim 12 nm$ from Fig. 2 c), and spectral gap of 3.8 mV, consistent with $E_C >$. This island could lie near either $q =$ or $q = e$, corresponding to an even or odd ground state, respectively, as shown in Fig. 2 d). Figure 5 d) demonstrates that this island lies, in fact, in an odd charge ground state by plotting the evolution of the spectral gap with B. The gap closes initially with B due to the suppression of the tip s superconductivity, whereas the subsequent reopening at higher fields demonstrates the reappearance of the larger Coulomb blockade gap as the island s superconductivity is quenched. This is the signature of an odd parity ground state stabilized in the island within a range of $q^{odd} = 1$ $/E_C$ around $q \pm e$, as shown in Fig. 2 d). In contrast, for larger islands [e.g., Fig. 2 b)] the gap remains constant with field, as $E_C <$ and $q =$, which stabilizes an even ground state.

Conclusions   In summary, we have shown that superconducting correlations compete with Coulomb blockade in lead islands with radius amounting to tens of nanometers. This interplay of interactions is detected as wider gaps in the density of states measured with scanning tunneling spectroscopy. We used a magnetic field to disentangle the different roles of electronic pairing and Coulomb effects in the gap and found a critical effective

radius amounting to 12 nm below which Coulomb blockade dominates and even-odd parity ground states coexist and can be tuned with electrostatic gating. In our work, we spanned a wide range of Coulomb blockade and superconducting pairing interactions controlled by the size of the particle, and tuned gating potential by applying voltage pulses. This allowed us to provide a convincing picture of the dominant role of Coulomb blockade in the destruction of superconductivity in small clusters. In combination with DBTJ model, we show that smaller clusters can stabilize odd-charge-parity superconducting ground states. The tunability of this versatile platform is ideal for exploring the design principles of -junction superconducting devices, with a promising role in the realization of topological qubits [44,53 55].

Data availability   The data that support the findings of this article are openly available [44], embargo periods may apply.

[1] P. W. Anderson, Theory of dirty superconductors, J. Phys. Chem. Solids **11**, 26 1959).

[2] A. L. Efros and B. I. Shklovskii, Coulomb gap and low temperature conductivity of disordered systems, J. Phys. C **8**, L49 1975).

[3] K. K. Likharev, Correlated discrete transfer of single electrons in ultrasmall tunnel junctions, IBM J. Res. Dev. **32**, 144 1988).

[4] H. Grabert and M. H. Devoret, eds., *Single Charge Tunneling*, NATO ASI Series, Vol. 294 Springer, Boston, MA, 1992).

[5] A. E. Hanna and M. Tinkham, Variation of the Coulomb staircase in a two-junction system by fractional electron charge, Phys. Rev. B **44**, 5919 1991).

[6] S. Vlaic, S. Pons, T. Zhang, A. Assouline, A. Zimmers, C. David, G. Rodary, J.-C. Girard, D. Roditchev, and H. Aubin, Superconducting parity effect across the Anderson limit, Nat. Commun. **8**, 14549 2017).

[7] B. L. Al tshuler, P. A. Lee, and R. A. Webb, *Mesoscopic Phenomena in Solids*, Modern Problems in Condensed

Matter Sciences No. v. 30 North Holland Sole distributors for the USA and Canada, Elsevier Science, Amsterdam, New York, 1991).

[8] G.-L. Ingold and Yu. V. Nazarov, Charge tunneling rates in ultrasmall junctions, in *Single Charge Tunneling*, Vol. 294, edited by H. Grabert and M. H. Devoret Springer, Boston, MA, 1992), pp. 21 107.

[9] D. V. Averin and K. K. Likharev, Coulomb blockade of single-electron tunneling, and coherent oscillations in small tunnel junctions, J. Low Temp. Phys. **62**, 345 1986).

[10] B. van Heck, R. M. Lutchyn, and L. I. Glazman, Conductance of a proximitized nanowire in the Coulomb blockade regime, Phys. Rev. B **93**, 235431 2016).

[11] T. Dittrich, ed., *Quantum Transport and Dissipation* Wiley-VCH, Weinheim; New York, 1998).

[12] K. A. Matveev, M. Gisselfält, L. I. Glazman, M. Jonson, and R. I. Shekhter, Parity-induced suppression of the Coulomb blockade of Josephson tunneling, Phys. Rev. Lett. **70**, 2940 1993).

[13] K. A. Matveev, L. I. Glazman, and R. I. Shekhter, Effects of charge parity in tunneling through a superconducting grain, Mod. Phys. Lett. B **08**, 1007 1994).

[14] J. von Delft, A. D. Zaikin, D. S. Golubev, and W. Tichy, Parity-affected superconductivity in ultrasmall metallic grains, Phys. Rev. Lett. **77**, 3189 1996).

[15] B. Sacépé, M. Feigel man, and T. M. Klapwijk, Quantum breakdown of superconductivity in low-dimensional materials, Nat. Phys. **16**, 734 2020).

[16] S. C. Ganguli, V. Vano, S. Kezilebieke, J. L. Lado, and P. Liljeroth, Confinement-engineered superconductor to correlated-insulator transition in a van der Waals monolayer, Nano Lett. **22**, 1845 2022).

[17] C. Carbillet, V. Cherkez, M. A. Skvortsov, M. V. Feigel man, F. Debontridder, L. B. Ioffe, V. S. Stolyarov, K. Ilin, M. Siegel, D. Roditchev, T. Cren, and C. Brun, Spectroscopic evidence for strong correlations between local superconducting gap and local Altshuler-Aronov density of states suppression in ultrathin NbN films, Phys. Rev. B **102**, 024504 2020).

[18] D. Badami, X-ray studies of graphite formed by decomposing silicon carbide, Carbon **3**, 53 1965).

[19] K. S. Novoselov, A. K. Geim, S. V. Morozov, D. Jiang, Y. Zhang, S. V. Dubonos, I. V. Grigorieva, and A. A. Firsov, Electric field effect in atomically thin carbon films, Science **306**, 666 2004).

[20] E. Cortés-del Río, J. L. Lado, V. Cherkez, P. Mallet, J.-Y. Veuillen, J. C. Cuevas, J. M. Gómez-Rodríguez, J. Fernández-Rossier, and I. Brihuega, Observation of Yu Shiba Rusinov states in superconducting graphene, Adv. Mater. **33**, 2008113 2021).

[21] E. Cortés-del Río, Stefano. Trivini, J. I. Pascual, V. Cherkez, P. Mallet, J.-Y. Veuillen, Juan. C. Cuevas, and I. Brihuega, Shaping graphene superconductivity with nanometer precision, Small **20**, 2308439 2024).

[22] S. Trivini, T. Kokkeler, J. Ortuzar, E. Cortés-del Río, B. Viña-Bausá, P. Mallet, J.-Y. Veuillen, J. C. Cuevas, I. Brihuega, F. S. Bergeret, and J. I. Pascual, From local to

collective superconductivity in proximitized graphene, Nano Lett. 2025), 10.1021/acs.nanolett.5c03487.

[23] B. Rachmilowitz, H. Zhao, Z. Ren, H. Li, K. H. Thomas, J. Marangola, S. Gao, J. Schneeloch, R. Zhong, G. Gu, C. Flindt, and I. Zeljkovic, Coulomb blockade effects in a topological insulator grown on a high-Tc cuprate superconductor, npj Quantum Mater. **5**, 72 2020).

[24] L. Serrier-Garcia, J. C. Cuevas, T. Cren, C. Brun, V. Cherkez, F. Debontridder, D. Fokin, F. S. Bergeret, and D. Roditchev, Scanning tunneling spectroscopy study of the proximity effect in a disordered two-dimensional metal, Phys. Rev. Lett. **110**, 157003 2013).

[25] SPECS Joule Thomson STM.

[26] C. Brun, K. H. Müller, I.-Po Hong, F. Patthey, C. Flindt, and W.-D. Schneider, Dynamical Coulomb blockade observed in nanosized electrical contacts, Phys. Rev. Lett. **108**, 126802 2012).

[27] R.-F. Wang, Y.-L. Xiong, H. Yan, X. Hu, M. Osada, D. Li, H. Y. Hwang, C.-L. Song, X.-C. Ma, and Q.-K. Xue, Observation of Coulomb blockade and Coulomb staircases in superconducting Pr 0.8 Sr 0.2 NiO 2 films, Phys. Rev. B **107**, 115411 2023).

[28] M. H. Devoret, D. Esteve, H. Grabert, G.-L. Ingold, H. Pothier, and C. Urbina, Effect of the electromagnetic environment on the Coulomb blockade in ultrasmall tunnel junctions, Phys. Rev. Lett. **64**, 1824 1990).

[29] See Supplemental Material at http://link.aps.org/supplemental/10.1103/vkwr-m87v for details on the model and additional data, which includes Refs. [30 43].

[30] W. Norimatsu and M. Kusunoki, Epitaxial graphene on SiC0001: Advances and perspectives, Phys. Chem. Chem. Phys. **16**, 3501 2014).

[31] J. G. Rodrigo, H. Suderow, and S. Vieira, On the use of STM superconducting tips at very low temperatures, Eur. Phys. J. B **40**, 483 2004).

[32] M. Tinkham, *Introduction to Superconductivity*, International Series in Pure and Applied Physics McGraw Hill, New York, 1996).

[33] M. Amman, R. Wilkins, E. Ben-Jacob, P. D. Maker, and R. C. Jaklevic, Analytic solution for the current-voltage characteristic of two mesoscopic tunnel junctions coupled in series, Phys. Rev. B **43**, 1146 1991).

[34] P. G. De Gennes and M. Tinkham, Magnetic behavior of very small superconducting particles, Physics Long Island City, N.Y.) **1**, 107 1964).

[35] J. Perenboom, P. Wyder, and F. Meier, Electronic properties of small metallic particles, Phys. Rep. **78**, 173 1981).

[36] C. T. Black, D. C. Ralph, and M. Tinkham, Spectroscopy of the superconducting gap in individual nanometer-scale aluminum particles, Phys. Rev. Lett. **76**, 688 1996).

[37] L. Schneider, P. Beck, J. Wiebe, and R. Wiesendanger, Atomic-scale spin-polarization maps using functionalized superconducting probes, Sci. Adv. **7**, eabd7302 2021).

[38] R. C. Dynes, V. Narayanamurti, and J. P. Garno, Direct measurement of quasiparticle-lifetime broadening in a strong-coupled superconductor, Phys. Rev. Lett. **41**, 1509 1978).

[39] J. Von Delft, Superconductivity in ultrasmall metallic grains, Ann. Phys. Berlin) **513**, 219 2001).

[40] G. Sierra, J. Dukelsky, G. G. Dussel, J. von Delft, and F. Braun, Exact study of the effect of level statistics in ultrasmall superconducting grains, Phys. Rev. B **61**, R11890 2000).

[41] F. Braun and J. von Delft, Fixed- N superconductivity: The crossover from the bulk to the few-electron limit, Phys. Rev. Lett. **81**, 4712 1998).

[42] M. Ruby, B. W. Heinrich, J. I. Pascual, and K. J. Franke, Experimental demonstration of a two-band superconducting state for lead using scanning tunneling spectroscopy, Phys. Rev. Lett. **114**, 157001 2015).

[43] D. V. Averin and Yu. V. Nazarov, Single-electron charging of a superconducting island, Phys. Rev. Lett. **69**, 1993 1992).

[44] S. Trivini, Available data attached to the publication: Local control of parity and charge in nanoscale superconducting lead islands, 10.5281/zenodo.17351235, 2025).

[45] T. M. Eiles, J. M. Martinis, and M. H. Devoret, Even-odd asymmetry of a superconductor revealed by the Coulomb blockade of Andreev reflection, Phys. Rev. Lett. **70**, 1862 1993).

[46] J. M. Hergenrother, M. T. Tuominen, and M. Tinkham, Charge transport by Andreev reflection through a mesoscopic superconducting island, Phys. Rev. Lett. **72**, 1742 1994).

[47] C. R. Ast, B. Jäck, J. Senkpiel, M. Eltschka, M. Etzkorn, J. Ankerhold, and K. Kern, Sensing the quantum limit in scanning tunnelling spectroscopy, Nat. Commun. **7**, 13009 2016).

[48] J. Senkpiel, J. C. Klöckner, M. Etzkorn, S. Dambach, B. Kubala, W. Belzig, A. L. Yeyati, J. C. Cuevas, F. Pauly, J. Ankerhold, C. R. Ast, and K. Kern, Dynamical Coulomb blockade as a local probe for quantum transport, Phys. Rev. Lett. **124**, 156803 2020).

[49] Y. Yuan, X. Wang, C. Song, L. Wang, K. He, X. Ma, H. Yao, W. Li, and Q.-K. Xue, Observation of Coulomb gap and enhanced superconducting gap in nano-sized Pb islands grown on SrTiO₃, Chin. Phys. Lett. **37**, 017402 2020).

[50] V. W. Brar, R. Decker, H.-M. Solowan, Y. Wang, L. Maserati, K. T. Chan, H. Lee, Ç. O. Girit, A. Zettl, S. G. Louie, M. L. Cohen, and M. F. Crommie, Gate-controlled ionization and screening of cobalt adatoms on a graphene surface, Nat. Phys. **7**, 43 2011).

[51] I.-P. Hong, C. Brun, M. Pivetta, F. Patthey, and W.-D. Schneider, Coulomb blockade phenomena observed in supported metallic nanoislands, Front. Phys. **1**, 13 2013).

[52] J. Shen, S. Heedt, F. Borsoi, B. van Heck, S. Gazibegovic, R. L. M. Op het Veld, D. Car, J. A. Logan, M. Pendharkar, S. J. J. Ramakers, G. Wang, D. Xu, D. Bouman, A. Geresdi, C. J. Palmstrøm, E. P. A. M. Bakkers, and L. P. Kouwenhoven, Parity transitions in the superconducting ground state of hybrid InSb Al Coulomb islands, Nat. Commun. **9**, 4801 2018).

[53] S. M. Albrecht, A. P. Higginbotham, M. Madsen, F. Kuemmeth, T. S. Jespersen, J. Nygård, P. Krogstrup, and C. M. Marcus, Exponential protection of zero modes in Majorana islands, Nature London) **531**, 206 2016).

[54] S. Plugge, A. Rasmussen, R. Egger, and K. Flensberg, Majorana box qubits, New J. Phys. **19**, 012001 2017).

[55] R. M. Lutchyn, E. P. A. M. Bakkers, L. P. Kouwenhoven, P. Krogstrup, C. M. Marcus, and Y. Oreg, Majorana zero modes in superconductor semiconductor heterostructures, Nat. Rev. Mater. **3**, 52 2018).